



TÜBİTAK

Turkish Journal of Physics

<http://journals.tubitak.gov.tr/physics/>

Research Article

Turk J Phys
(2016) 40: 181 – 200
© TÜBİTAK
doi:10.3906/fiz-1509-17

Properties of asymmetric semiinfinite nuclear systems in the extended Thomas–Fermi model

Mohamed ABD-ALLA*

Department of Physics, Faculty of Science, Cairo University, Giza, Egypt

Received: 14.09.2015

Accepted/Published Online: 13.04.2015

Final Version: 01.12.2016

Abstract: We start from the energy density of the Skyrme interaction and perform a leptodermous expansion for an asymmetric semiinfinite nuclear system. We get a liquid drop model formula for the energy of such a system. We use the obtained analytic formulae for volume, surface, and curvature energies to study the properties of asymmetric nuclear systems. We also study the effect of the asymmetry parameter on the volume, surface, and curvature properties.

Key words: Nuclear structure, extended Thomas–Fermi model, semiinfinite nuclear matter, liquid drop model expansion, incompressibility

1. Introduction

Understanding the properties of hot asymmetric nuclear matter has an important impact on the study of nuclear structure close to drip lines [1], of astrophysical processes [2], and of heavy ion reaction mechanisms [3]. Being a quantal system, the atomic nucleus is best described by the shell model or one of its self-consistent versions, such as Hartree–Fock or random phase approximations. However, a fairly good description of the nucleus can be obtained with a semiclassical approach such as the droplet model [4–7] or the extended Thomas–Fermi model [8,9], which includes the correlations given by the Pauli principle but ignores quantal oscillations. It was shown that the extended Thomas–Fermi model numerically yields the same results as the microscopical Hartree–Fock approach [10–12] for temperatures larger than 3 MeV, where the shell effects disappear. In the limit of very large spherical nuclei, the density profile across the surface becomes that of semiinfinite nuclear matter. This is a one-dimensional geometry with the density varying along one axis and extending to infinity in the two other directions. Assuming the nuclear density to be flat in the interior and to vary only in a relatively narrow surface region (a leptodermous system), the total energy of a spherical nucleus is expanded into volume, surface, curvature, and higher order contributions [4–7]. Leptodermous expansion of the nuclear energy has proved enormously useful in calculating fission barriers, ground-state masses and deformations, and other nuclear properties [8]. Within a context related to the liquid drop model (LDM) and the leptodermous expansion of a finite nucleus, the surface and curvature energy coefficients can be extracted from semiinfinite nuclear matter [13–15]. This schematic geometry avoids undesired shell, Coulomb, and finite-size effects, which makes it very appropriate to study surface properties.

In the present work, we used Skyrme parameterizations for the energy density (in the framework of the extended Thomas–Fermi model) and got a LDM formula for the total energy of asymmetric semiinfinite nuclear

*Correspondence: mabdallah@sci.cu.edu.eg

matter (ASINM). The surface and curvature energies have analytical formulae. Such formulae are needed in calculations of supernovae formation [2,16] and the fragmentation of hot compound nuclei [17,18]. We used these formulae to study surface and curvature properties of ASINM. In Section 2, we present our model calculations for the LDM expansion of ASINM systems. In Section 3, we present our results and discussion. We presented a summary and conclusions in Section 4.

2. Model calculations

The total energy of a nucleus is:

$$E = \int H(r)dr \quad (1)$$

where $H(r)$ is the Hamiltonian density, which contains a nuclear part and a Coulomb part. Here we neglect the Coulomb part. For the nuclear part, we shall use the energy density obtained with Skyrme-type forces. For even-even nuclei (neglecting the spin-orbit term), the Skyrme energy density takes the following explicit form [8]:

$$\begin{aligned} H(r) = & \frac{\hbar^2}{2m}\tau + \frac{1}{2}t_0[(1 + \frac{1}{2}x_0)\rho^2 - (\frac{1}{2} + x_0)(\rho_n^2 + \rho_p^2)] \\ & + \frac{1}{12}t_3\rho^\alpha[(1 + \frac{1}{2}x_3)\rho^2 - (\frac{1}{2} + x_3)(\rho_n^2 + \rho_p^2)] \\ & + \frac{1}{4}[t_1(1 + \frac{1}{2}x_1) + t_2(1 + \frac{1}{2}x_2)]\rho\tau + \frac{1}{4}[t_2(\frac{1}{2} + x_2) - t_1(\frac{1}{2} + x_1)](\rho_n\tau_n + \rho_p\tau_p) \\ & - \frac{1}{16}[3t_1(1 + \frac{1}{2}x_1) + t_2(1 + \frac{1}{2}x_2)](\nabla\rho)^2 + \frac{1}{16}[3t_1(1 + \frac{1}{2}x_1) - t_2(1 + \frac{1}{2}x_2)][(\nabla\rho_n)^2 + (\nabla\rho_p)^2] \end{aligned} \quad (2)$$

where ρ ($\rho = \rho_n + \rho_p$) is the local density, τ ($\tau = \tau_n + \tau_p$) is the kinetic energy density, and $t_0, t_1, t_2, t_3, x_0, x_1, x_2, x_3$, and α are the interaction parameters.

For the kinetic energy density, we used the extended Thomas–Fermi model (see references [8,9] for details):

$$\tau_q(\rho) = \tau_{0q}(\rho) + \tau_{2q}(\rho) + \tau_{4q}(\rho) \quad (3)$$

where τ_{0q} is the standard Thomas–Fermi kinetic energy density and q refers to a neutron or a proton. It is given by:

$$\tau_{0q}(\rho) = \frac{3}{5} \left(\frac{3\pi^2\rho_q}{2} \right)^{\frac{3}{2}} \quad (4)$$

$\tau_{2q}(\rho)$ is the second-order correction and is given by:

$$\tau_{2q}(\rho) = \frac{1}{36} \frac{(\nabla\rho_q)^2}{\rho_q} + \frac{1}{3}\Delta\rho_q + \frac{1}{6}\frac{\nabla\rho_q \cdot \nabla f_q}{f_q} + \frac{1}{6}\frac{\rho_q \nabla f_q}{f_q} - \frac{1}{12}\rho_q \left(\frac{\nabla f_q}{f_q} \right)^2 \quad (5)$$

$\tau_{4q}(\rho)$ is the fourth-order correction and is given by:

$$\tau_{4q}(\rho_q) = \frac{1}{6480} \left(\frac{2}{3\pi^2} \right)^{\frac{2}{3}} \rho_q^{\frac{1}{3}} \left\{ 8 \left(\frac{\nabla\rho_q}{\rho_q} \right)^4 - 27 \left(\frac{\nabla\rho_q}{\rho_q} \right)^2 \left(\frac{\Delta\rho_q}{\rho_q} \right) - 24 \left(\frac{\Delta\rho_q}{\rho_q} \right)^2 \right\} \quad (6)$$

The relation that relates the function f_q to effective mass is:

$$f_q = \frac{m}{m_q^*} = 1 + \frac{\partial H}{\partial \tau_q} \quad (7)$$

This gives:

$$f_q = 1 + \frac{m}{2\hbar^2} \{ [t_1(1 + 0.5x_1) + t_2(1 + 0.5x_2)] \rho - [t_1(1 + 0.5x_1) - t_2(1 + 0.5x_2)] \rho_q \} \quad (8)$$

In the asymptotic limit of a very heavy nucleus the surface diffusion of the local density is much smaller than the radius R at which the surface is located. In this case, we can approximate the finite nucleus by the so-called semiinfinite nuclear matter (SINM). In order to determine the energy of SINM, we assume the density profile to be a Fermi distribution with a power. This choice has been found to give a very good approximation to the exact solution of the Euler–Lagrange variational equations [9,19]. The neutron and proton density profiles for SINM take the following form:

$$\rho_q(r) = \rho_{0q} \left[1 + \exp\left(\frac{r - R_q}{d}\right) \right]^{-\nu} \quad (9)$$

where ρ_{0q} is the nucleon density deep inside the system, R_q is the half-value radius, d is the diffuseness parameter, and ν is a power.

For simplicity we neglect the neutron skin, i.e. $R_n = R_p = R$. The zero neutron-skin assumption is applicable for SINM and for ordinary even-even nuclei. Using the Fermi distribution for the density profile, the energy equation reduces to integrations of the following form:

$$\int_0^\infty \rho_q^s(r) dr, \int_0^\infty \rho_q^{-s}(r) dr \text{ and } \int_0^\infty \rho_q^s(r) \rho_p^s(r) dr \quad (10)$$

Srivastava [20] found a formula for the integration $\int_0^\infty \rho_q^s(r) dr$ and the result is:

$$\int_0^\infty \rho_q^s(r) dr = \frac{4\pi}{3} \rho_{0q}^s [R^3 - 3R^2 d A_1(sv) + 6Rd^2 A_2(sv) - 6d^3 A_3(sv)] \quad (11)$$

where the coefficients $A_n(s)$ are given by:

$$A_n(s) = \frac{1}{(n-1)!} \int_0^\infty [1 - (1+e^{-x})^q + (-1)^n (1+e^{-x})^{-q}] x^{n-1} dx \quad (12)$$

The integrations $\int_0^\infty \rho_q^s(r) \rho_p^s(r) dr$ were derived by Abd-Alla et al. [14] in the following form:

$$\int_0^\infty \rho_q^s(r) \rho_p^p(r) dr = \frac{4\pi}{3} \rho_{0q}^s \rho_{0p}^p [R^3 - 3R^2 d A_1((s+p)v) + 6Rd^2 A_2((s+p)v) - 6d^3 A_3((s+p)v)] \quad (13)$$

The integrations $\int_0^\infty \rho_q^{-s}(r) dr$ were derived by Abd-Alla [21] in the following form:

$$\int_0^\infty \rho_q^{-s}(r) dr = \frac{4\pi}{3} \rho_{0q}^{-s} [R^3 - 3R^2 d B_1(sv) + 6Rd^2 B_2(sv) - 6d^3 B_3(sv)] \quad (14)$$

The coefficients $B_n(s)$ are given in reference [21] (see reference [21] for details).

The normalization condition

$$\int_0^\infty \rho(r)dr = A = \frac{4\pi}{3}\rho_0[R^3 - 3R^2dA_1(v) + 6Rd^2A_2(v) - 6d^3A_3(v)] \quad (15)$$

is inverted to write the radius R in terms of the mass number A and we get:

$$R = \left(\frac{3A}{4\pi\rho_0}\right)^{\frac{1}{3}} - \frac{\pi^2 d^2}{3} \left(\frac{3A}{4\pi\rho_0}\right)^{-\frac{1}{3}} \quad (16)$$

Applying these simplifications, we get the leptodermous expansion for the energy (the LDM formula) of the system in the following form:

$$\frac{E(\rho, X)}{A} = E_v(\rho, X) + E_s(\rho, X)A^{-\frac{1}{3}} + E_c(\rho, X)A^{-\frac{2}{3}} \quad (17)$$

$E_v(\rho, X)$ is the volume energy, $E_s(\rho, X)$ is the surface energy, and $E_c(\rho, X)$ is the curvature energy. X is the asymmetry parameter defined by:

$$X = \frac{\rho_{0n} - \rho_{0p}}{\rho_0} \quad (18)$$

In the present work, we expand the total energy in X up to X^2 . Recent theoretical studies [22,23] showed that X^4 and X^6 expansion had a negligible effect on the energy of the system. This is suitable and expected for studying heavy nuclei near the stability line.

The volume energy in X^2 approximation is:

$$E_v(\rho, X) = E_{v0} + X^2 E_{vx} \quad (19)$$

where E_{v0} is the bulk volume energy and E_{vx} is the symmetry volume energy.

The bulk volume energy E_{v0} is given by:

$$E_{v0} = \frac{3}{5}\left(\frac{\hbar^2}{2m^*}\right)\left(\frac{3\pi^2\rho}{2}\right)^{2/3} + \frac{3}{8}t_0\rho + \frac{1}{16}t_3\rho^{\alpha+1} + \frac{3}{80}\left(\frac{3\pi^2}{2}\right)^{2/3}\rho^{5/3}(3t_1 + 5t_2 + 4t_2x_2) \quad (20)$$

The symmetry volume energy E_{vx} is given by:

$$E_{vx} = \frac{1}{3}\left(\frac{\hbar^2}{2m^*}\right)\left(\frac{3\pi^2}{2}\right)^{2/3}\rho^{2/3} - \frac{1}{8}t_0\rho(1 + 2x_0) - \frac{1}{48}t_3\rho^{\alpha+1}(1 + 2x_3) + \frac{1}{24}\left(\frac{3\pi^2}{2}\right)^{2/3}\rho^{5/3}(4t_2 - 3t_1x_1 + 5t_2x_2) \quad (21)$$

The surface energy is:

$$E_s(\rho, X) = E_{s0} + X^2 E_{sx} \quad (22)$$

where E_{s0} is the bulk surface energy and E_{sx} is the symmetry surface energy.

The bulk surface energy E_{s0} and the symmetry surface energy E_{sx} have long analytical formulae and they are given in the Appendix.

The curvature energy is given by:

$$E_c(\rho, X) = E_{c0}(\rho) + X^2 E_{cx}(\rho) \quad (25)$$

where E_{c0} is the bulk curvature energy and E_{cx} is the curvature symmetry energy.

The bulk curvature energy E_{c0} and the symmetry curvature energy E_{cx} have long analytical formulae and they are given in the Appendix.

The pressure (P), incompressibility (K), energy slope parameters (L), and skewness parameter (Q) are defined by:

$$\begin{aligned} P &= \rho^2 \frac{\partial E}{\partial \rho}, \\ K &= 9 \frac{\partial P}{\partial \rho}, \\ L &= 3\rho \frac{\partial E}{\partial \rho} \end{aligned} \quad (30)$$

and

$$Q = 27\rho^3 \frac{\partial^3 E}{\partial \rho^3}$$

Using the analytical equations for the volume, surface, and curvature terms, we got the LDM expansion for these quantities.

For the total pressure P of the system, we got:

$$P = (P_{v0} + P_{vx}X^2) + (P_{s0} + P_{sx}X^2)A^{-\frac{1}{3}} + (P_{c0} + P_{cx}X^2)^{-\frac{2}{3}} \quad (31)$$

P_{v0} (P_{s0} , P_{c0}) is the bulk volume (bulk surface, bulk curvature) pressure and P_{vx} (P_{sx} , P_{cx}) is the symmetry volume (symmetry surface, symmetry curvature) pressure.

For the incompressibility K of the system, we got:

$$K = (K_{v0} + K_{vx}X^2) + (K_{s0} + K_{sx}X^2)A^{-\frac{1}{3}} + (K_{c0} + K_{cx}X^2)^{-\frac{2}{3}} \quad (32)$$

K_{v0} (K_{s0} , K_{c0}) is the bulk volume (bulk surface, bulk curvature) incompressibility and K_{vx} (K_{sx} , K_{cx}) is the symmetry volume (symmetry surface, symmetry curvature) incompressibility.

For the energy slope parameter L, we got:

$$L = (L_{v0} + L_{vx}X^2) + (L_{s0} + L_{sx}X^2)A^{-\frac{1}{3}} + (L_{c0} + L_{cx}X^2)^{-\frac{2}{3}} \quad (33)$$

L_{v0} (L_{s0} , L_{c0}) is the bulk volume (bulk surface, bulk curvature) term and L_{vx} (L_{sx} , L_{cx}) is the symmetry volume (symmetry surface, symmetry curvature) term.

For the skewness parameter Q, we got:

$$Q = (Q_{v0} + Q_{vx}X^2) + (Q_{s0} + Q_{sx}X^2)A^{-\frac{1}{3}} + (Q_{c0} + Q_{cx}X^2)^{-\frac{2}{3}} \quad (34)$$

Q_{v0} (Q_{s0} , Q_{c0}) is the bulk volume (bulk surface, bulk curvature) term and Q_{vx} (Q_{sx} , Q_{cx}) is the symmetry volume (symmetry surface, symmetry curvature) term.

3. Results and discussion

In this section, we present our results for the volume, surface, and curvature properties in separate subsections and then discuss the properties of ASINM systems. We apply our calculations to the famous and more recent Skyrme parameterizations (there are about 240 parameterizations on the market [24,25]) and pay attention to the KDE0v1, LNS, NRAPR, SKRA, and SQMC700 parameterizations, which passed the macroscopic and microscopic constraints proposed by Dutra et al. [24]. We pay special attention to the LNS parameterization as it has average behavior (in our results) for most Skyrme parameterizations. For the density parameters (d , ν), we found that the surface energy has a minimum value with respect to the variations in these parameters. Table 1 shows the density parameters at the minimum surface energy for different Skyrme parameterizations.

We noticed that a value of $d = 0.552$ fm and $\nu = 1.24$ is suitable for all Skyrme parameterizations, which has a slight difference in the calculated surface ($E_{s0} \pm 1$ MeV) and curvature ($E_{c0} \pm 0.5$ MeV) energies

3.1. Volume properties

3.1.1. Volume energy

Figure 1 shows the behavior of the bulk volume energy with the relative density (ρ/ρ_0) for some Skyrme parameterizations. We found that all Skyrme parameterizations we considered have the same behavior with a slightly different value for the bulk volume energy. Figure 2 shows the behavior of the symmetry volume energy with the relative density. We notice that for densities ($\rho < \rho_0$) all Skyrme parameterizations have the same linear increasing behavior with the relative density. The volume symmetry energy will saturate at densities ($\rho \approx 3 \rho_0$) for most Skyrme parameterizations. Some Skyrme parameterizations (such as SKT9) saturate at ($\rho \approx 1.7 \rho_0$) and some do not show any saturation (such as SKxs25). This behavior reflects the constraint put on Skyrme parameterizations through the value of the symmetry volume energy slope (L_{vx}) at saturation [24]. The value of L_{vx} as determined from double differences of symmetry energies was estimated from experimental nuclear masses [26] to be 58.91 ± 1.08 MeV. A recent effort aided by microscopic calculations on the Δr_{np} of heavy nuclei [27–29] gave $L_{vx} = 59 \pm 13$ MeV. More recent experimental data on the values of Δr_{np} in ^{48}Ca , ^{132}Sn , and ^{208}Pb nuclei [30] gave $L_{vx} = 55.63 \pm 7$. Our result of calculations of L_{vx} for SKT9 is $L_{vx} = 33.75$ MeV, which is too small, and for SKxs25 it is $L_{vx} = 98.8$ MeV, which is too large. The effect of the asymmetry parameter X on the volume energy is to increase its value and slightly increase the saturation density. Figure 3 shows this behavior for LNS Skyrme parameterization. We found typical behavior for the other Skyrme parameterizations.

3.1.2. Volume pressure

The bulk volume pressure has the same behavior with the relative density as the bulk volume energy as shown in Figure 4. We noticed that all Skyrme parameterizations have a minimum bulk volume pressure at $\rho \approx 0.65 \rho_0$. The symmetry volume pressure (as shown in Figure 5) reflects the same behavior of the symmetry volume energy with the relative density discussed before. All Skyrme parameterizations reveal saturation at densities $1.5 \rho_0 < \rho < 2.5 \rho_0$ except for SKT9 parameterization, which saturates at $\rho \approx 1.2 \rho_0$, and SKxs25, which increases linearly with density. The constraint on L_{vx} shows the odd behavior of P_{vx} for SKT9 and SKxs25 parameterizations. Figure 6 shows the effect of the asymmetry parameter on the volume pressure for LNS parameterization. The effect of the asymmetry parameter X on the volume pressure is to increase its value and slightly increase the saturation density. We found typical behavior for the other Skyrme parameterizations.

Table 1. The density parameters (d , ν) at the minimum surface energy for different Skyrme parameterizations.

Skyrme force [ref.]	d (fm)	ν
BSK3 [35]	0.566	1.32
BSK7 [36]	0.563	1.32
BSK16 [37]	0.558	1.33
BSK17 [38]	0.560	1.33
KDE [39]	0.525	1.40
KDEOv1 [39]	0.530	1.41
MSK5 [40]	0.535	1.42
MSK6 [40]	0.540	1.39
MSL0 [41]	0.538	1.25
SK255 [42]	0.522	1.33
SK272 [42]	0.525	1.30
SKa25s20 [24]	0.530	1.20
SKa35s20 [24]	0.528	1.25
SKI3 [43]	0.535	1.36
SKI4 [43]	0.530	1.40
SKM* [8]	0.604	1.33
SKMP [44]	0.562	1.27
SKP [45]	0.552	1.20
SKSC6 [46]	0.533	1.44
SKT1 [47]	0.534	1.28
SKT2 [48]	0.531	1.30
SKT3 [48]	0.533	1.29
SKT9 [47]	0.537	1.24
SKX [48]	0.528	1.42
SKXce [48]	0.528	1.40
SKXm [48]	0.530	1.44
SKxs20 [49]	0.543	1.21
SKxs25 [49]	0.538	1.26
SLY6 [50]	0.548	1.18
SQMC650 [51]	0.542	1.25
SQMC700 [51]	0.547	1.20
SKRA [52]	0.538	1.37
LNS [53]	0.556	1.41
NPAPR [54]	0.558	1.40
v070 [55]	0.548	1.39
SV-SYM23 [56]	0.552	1.20
SV-min [56]	0.551	1.24
SAMi [33]	0.540	1.15

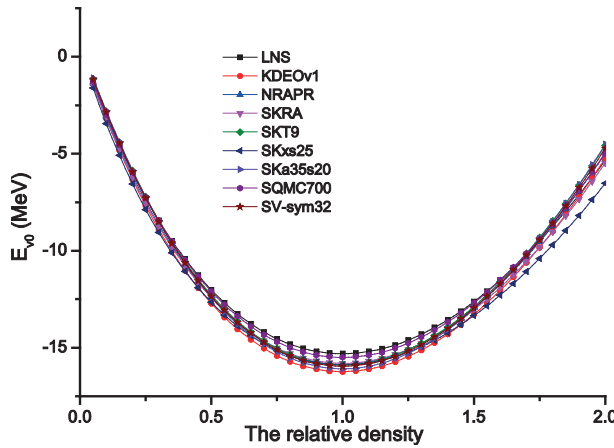


Figure 1. The dependence of bulk volume energy on relative density (ρ / ρ_0) for some Skyrme parameterizations.

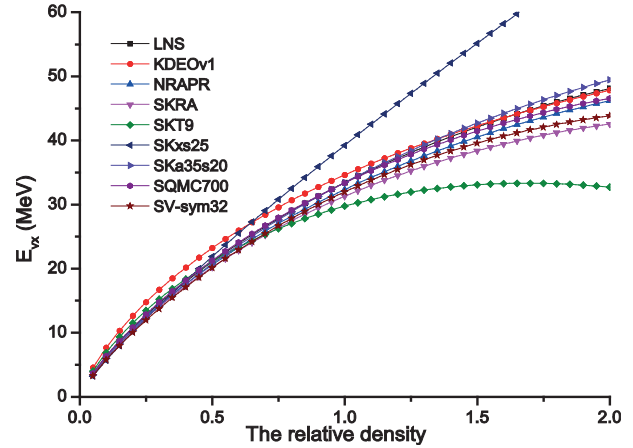


Figure 2. The dependence of symmetry volume energy on relative density (ρ / ρ_0) for some Skyrme parameterizations.

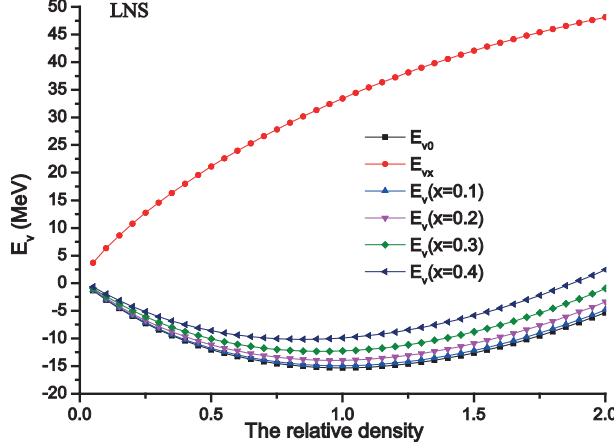


Figure 3. The effect of asymmetry parameter X on volume energy for LNS parameterization.

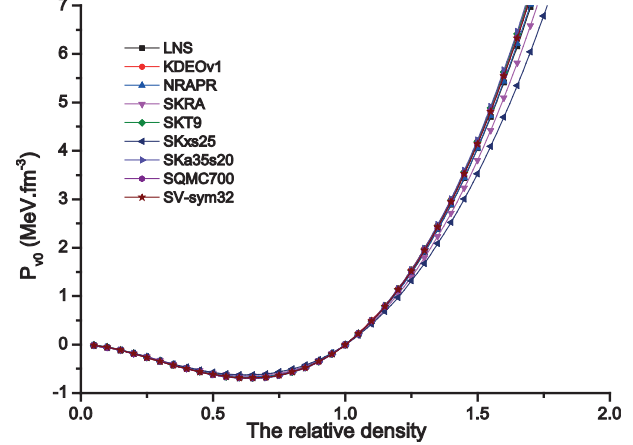


Figure 4. The dependence of bulk volume pressure on relative density (ρ / ρ_0) for some Skyrme parameterizations.

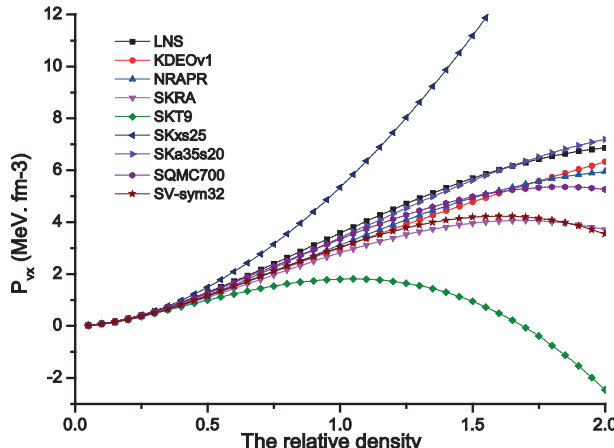


Figure 5. The dependence of symmetry volume pressure on relative density (ρ / ρ_0) for some Skyrme parameterizations.

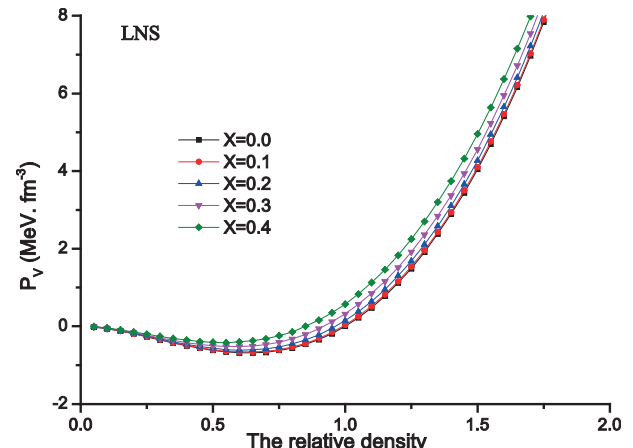


Figure 6. The effect of asymmetry parameter X on volume pressure for LNS parameterization.

3.1.3. Volume incompressibility

Figure 7 shows the rapidly increasing behavior of the bulk volume incompressibility with the relative density. We also noticed that all Skyrme parameterizations have the same value of bulk volume incompressibility at low densities ($\rho < 0.65 \rho_0$). For densities $0.65 \rho_0 > \rho \approx \rho_0$ the values of the bulk volume incompressibility for Skyrme parameterizations are closer and for densities $\rho > \rho_0$ these values become more and more different with increasing densities. Figure 8 shows the behavior of symmetry volume incompressibility with relative density. The SKT9 parameterization shows a rapidly decreasing behavior for the symmetry volume incompressibility with density, while SKxs25 shows a slow decreasing behavior. Again, the constraint on L_{vx} shows the odd behavior of K_{vx} for SKT9 and SKxs25 parameterizations. The main properties of infinite nuclear matter (volume properties) at saturation ($\rho = \rho_0$) are shown in Table 2 for some Skyrme potentials. The parameter L was defined in the droplet model [4–7] as the slope of the symmetry volume energy at saturation. This is the definition of L_{vx} in our model calculations. The skewness parameter (Q_{v0}) defined for the bulk volume term has the same definition as the droplet model parameter (Q). Here we have a new skewness parameter (Q_{vx}) that corresponds to the symmetry volume term.

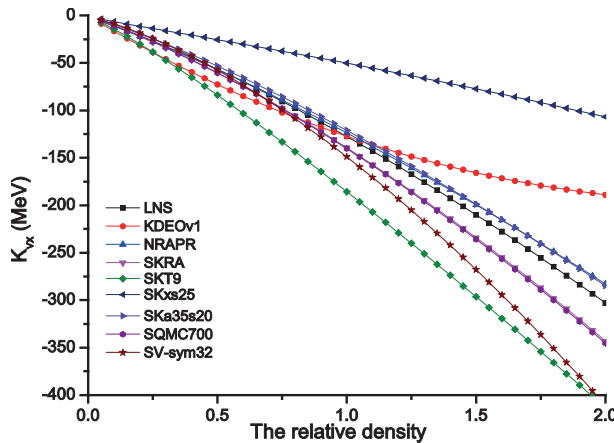


Figure 7. The dependence of bulk volume incompressibility on relative density (ρ / ρ_0) for some Skyrme parameterizations.

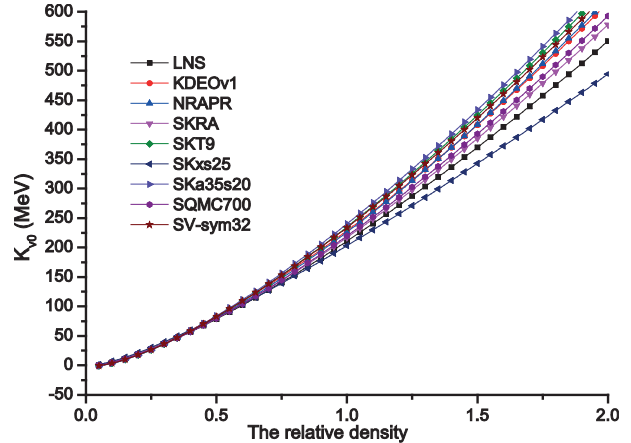


Figure 8. The dependence of symmetry volume incompressibility on relative density (ρ / ρ_0) for some Skyrme parameterizations.

3.2. Surface properties

3.2.1. Surface energy

Figure 9 shows the behavior of the bulk surface energy with relative density. We note that the surface energy increases with density and reaches its maximum value at a relative density $\rho \approx 0.75 \rho_0$ and then decreases to reach its zero value at $\rho \approx 1.65 \rho_0$. We correlate this behavior to the bulk volume pressure as follows: the bulk volume pressure decreases with density, reaches its minimum value at a relative density $\rho \approx 0.75 \rho_0$, and then increases slowly up to $\rho \approx 1.65 \rho_0$, above which it increases very rapidly. The maximum surface energy occurs at the minimum bulk volume pressure but not at the zero bulk volume pressure, which occurs at $\rho = \rho_0$. Figure 10 shows the symmetry surface energy as a function of the relative density. We notice that the symmetry surface energy at saturation is negative for some Skyrme parameterizations and is positive for others, and its value is not convergent for most Skyrme parameterizations. This may be due to the process of

Table 2. The main volume properties of infinite nuclear matter at saturation ($\rho = \rho_0$).

Skyrme force	E_{v0}	E_{vx}	L_{vx}	P_{vx}	K_{v0}	K_{vx}	Q_{v0}	Q_{vx}
BSK3	-15.80	27.93	6.75	0.35	234.8	-307.0	-380.8	550.4
BSK7	-15.75	28.00	16.87	0.89	229.1	-215.1	-370.6	603.4
BSK16	-16.05	30.00	34.88	1.84	241.8	-187.4	-363.7	462.0
BSK17	-16.05	30.00	36.29	1.92	241.7	-181.8	-363.5	450.4
KDE	-16.11	33.03	45.31	2.43	229.2	-144.9	-374.2	523.9
KDEOv1	-16.11	34.41	54.46	2.98	225.8	-126.2	-381.7	481.7
MSK5	-15.79	28.00	7.57	0.40	231.2	-282.6	-385.3	608.0
MSK6	-15.79	28.43	11.14	0.58	231.0	-273.5	-385.0	589.8
MSL0	-15.88	30.00	60.17	3.19	228.2	-98.7	-377.3	222.7
SAMi	-15.93	28.18	43.72	2.31	245.1	-120.0	-338.9	372.0
SK255	-16.33	37.38	95.01	4.98	254.8	-58.3	-349.9	94.2
SK272	-16.27	37.41	91.69	4.75	271.7	-67.8	-305.6	134.5
SKa25s20	-16.07	34.17	65.06	3.48	220.8	-117.8	-413.4	313.3
SKa35s20	-16.07	33.48	64.43	3.39	240.3	-120.9	-378.6	285.8
SKI3	-15.97	34.81	100.46	5.28	258.2	73.1	-303.8	211.5
SKI4	-15.93	29.51	60.46	3.22	247.8	-40.4	-330.9	350.7
SKM*	-15.77	30.03	45.76	2.45	216.6	-156.0	-386.1	330.5
SKMP	-15.55	29.88	70.30	3.68	230.8	-49.8	-338.0	159.4
SKP	-15.95	30.00	19.37	1.05	201.7	-267.8	-437.2	510.3
SKSC6	-15.94	24.63	11.18	0.60	235.6	-226.2	-382.5	501.8
SKT1	-15.98	31.68	55.13	2.96	236.1	-135.0	-383.5	319.4
SKT2	-15.94	31.66	55.11	2.96	235.7	-134.8	-382.6	319.0
SKT3	-15.94	31.41	54.81	2.94	235.7	-133.0	-382.7	315.3
SKT9	-15.88	29.76	33.75	1.80	234.9	-185.6	-371.0	472.0
SKX	-16.05	31.08	33.20	1.72	270.7	-251.9	-296.9	379.3
SKXce	-15.86	30.14	33.46	1.73	268.2	-238.4	-294.5	357.0
SKXm	-16.04	31.19	32.06	1.70	238.0	-242.8	-380.3	428.7
SKxs20	-15.78	36.25	69.77	3.76	201.9	-120.4	-425.0	325.4
SKxs25	-15.88	39.14	98.80	5.30	202.1	-50.0	-424.1	145.3
SLY6	-15.91	32.20	48.20	2.55	229.8	-112.4	-360.1	511.0
SQMC650	-15.57	33.66	52.92	3.03	218.2	-173.2	-376.9	349.8
SQMC700	-15.48	33.41	59.00	3.35	219.8	-140.4	-368.3	312.9
SKRA	-15.79	31.32	53.04	2.82	217.0	-139.3	-378.9	310.9
LNS	-15.31	33.43	61.45	3.58	210.9	-127.4	-382.7	302.6
NPAPR	-15.86	32.78	59.21	3.19	225.5	-123.8	-363.3	311.1
vo70	-15.78	27.83	-4.62	-0.24	231.2	-364.7	-385.3	595.4
SV-SYM23	-15.94	32.00	57.04	3.03	233.9	-148.9	-380.2	257.8
SV-min	-15.91	30.67	44.80	2.41	222.0	-156.7	-403.5	389.9

fitting the parameters of Skyrme forces, which did not take into account a property that is in direct relation with the symmetry surface energy of finite nuclei. Some calculations [31] deduced the symmetry surface energy by calculating the total symmetry energy of finite nuclei numerically and then subtracting the well-known value of the symmetry volume energy. Their resulting value for the symmetry surface energy, using some Skyrme parameterizations, is ($-33 \text{ MeV} \leq E_{sx} \leq -77 \text{ MeV}$). Other calculations based on fitting atomic masses in a LDM formula [32] gave a value for the symmetry surface energy of ($28 \text{ MeV} \leq E_{sx} \leq 45 \text{ MeV}$). These values, together with our divergent values, for the symmetry surface energy reflects the need of refitting the parameters of Skyrme interaction and taking into account a property that is in direct relation with the symmetry surface energy of finite nuclei. In Ref. [31] the authors extracted the macroscopic LDM parameters by using a large sample of finite spherical nuclei, including huge systems having $10^5\text{--}10^6$ nucleons, based on the self-consistent Skyrme–Hartree–Fock and relativistic mean field approach. They extracted the macroscopic information from the large-scale trends by subtracting fluctuating shell corrections and the Coulomb force was switched off to allow computation of very large nuclei. The methods used by the authors of references [31] and [32] are based on numerical fitting techniques, while our method is based on deriving analytical formulae for the LDM coefficients. The effect of the asymmetry parameter X on the surface energy is to increase its value and slightly increase the saturation density. Figure 11 shows this behavior for LNS Skyrme parameterization. We found a typical behavior for the other Skyrme parameterizations.

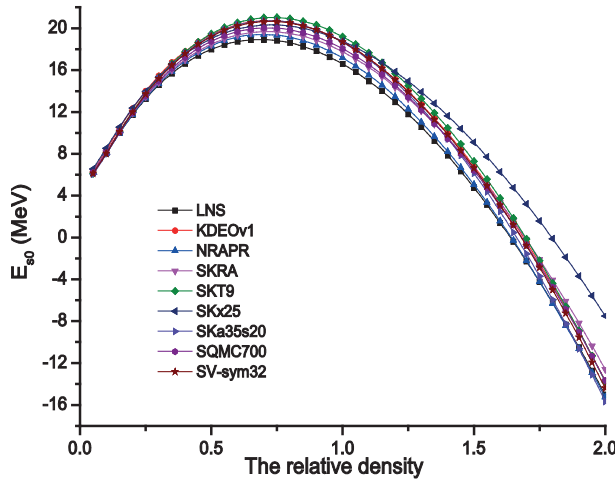


Figure 9. The dependence of bulk surface energy on relative density (ρ / ρ_0) for some Skyrme parameterizations.

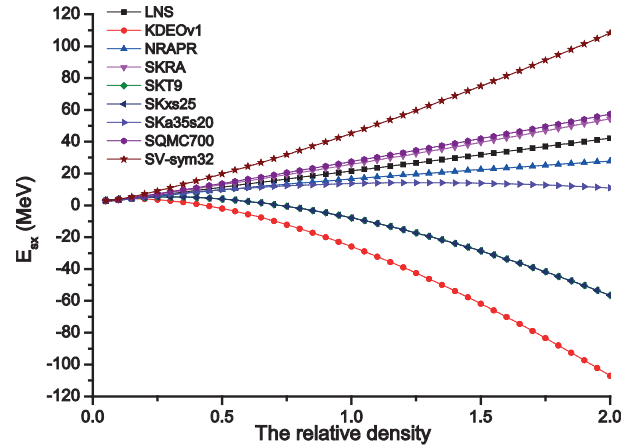


Figure 10. The dependence of symmetry surface energy on relative density (ρ / ρ_0) for some Skyrme parameterizations.

3.2.2. Surface pressure

The bulk surface pressure is shown in Figure 12. We note that the bulk surface pressure is zero for densities $\rho \leq 0.65 \rho_0$ and then monotonically decreases to high negative values (except for the NRAPR parameterization, which has an inflection point at $\rho \approx 1.8 \rho_0$). This behavior may be correlated to the bulk volume pressure, which has small negative values for densities $\rho \leq 0.65 \rho_0$ and then monotonically increases to high positive values. The symmetry surface pressure is shown in Figure 13. The behavior of the symmetry surface pressure is divergent for different Skyrme parameterizations and reflects the divergent behavior of the symmetry surface energy. The effect of the asymmetry parameter X on the surface energy is to increase its value and slightly

increase the saturation density. Figure 14 shows this behavior for LNS Skyrme parameterization. We found typical behavior for the other Skyrme parameterizations. The effect of asymmetry parameter X on the surface pressure is negligible, as seen in Figure 14.

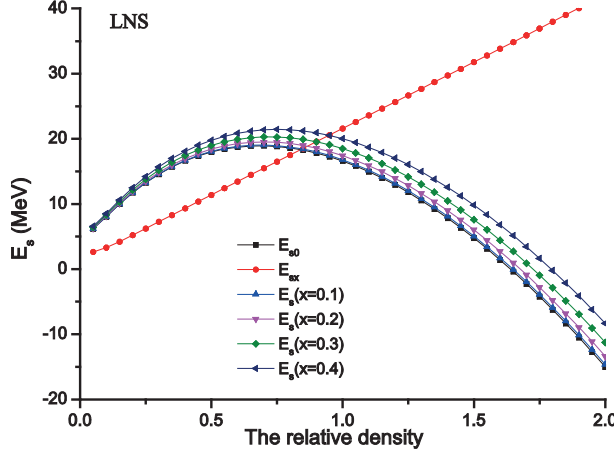


Figure 11. The effect of asymmetry parameter X on surface energy for LNS parameterization.

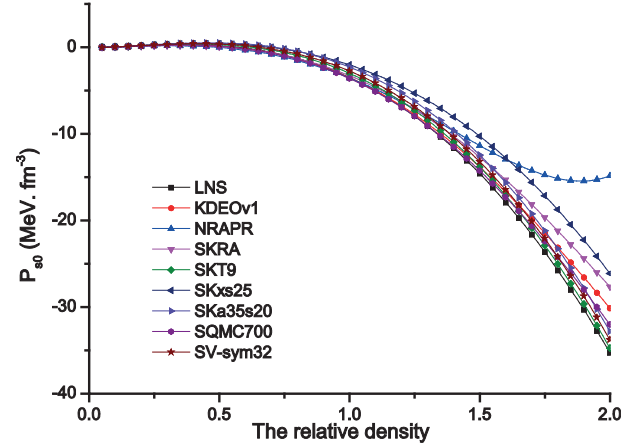


Figure 12. The dependence of bulk surface pressure on relative density (ρ / ρ_0) for some Skyrme parameterizations.

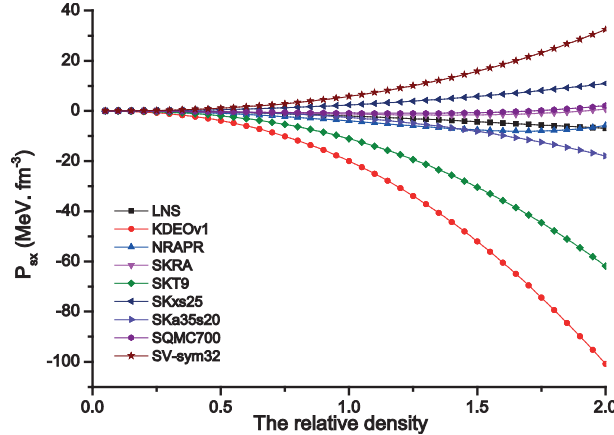


Figure 13. The dependence of symmetry surface pressure on relative density (ρ / ρ_0) for some Skyrme parameterizations.

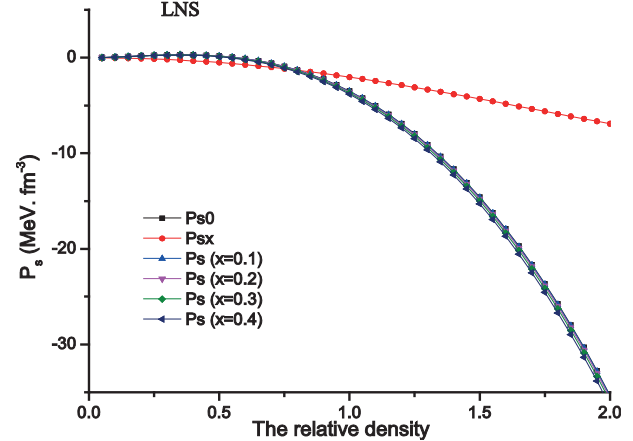


Figure 14. The effect of asymmetry parameter X on surface pressure for LNS parameterization.

3.2.3. Surface incompressibility

Figure 15 shows the bulk surface incompressibility for some Skyrme parameterizations. The bulk surface incompressibility decreases with density to high negative values (except for the NRAPR parameterization, which has an inflection point at $\rho \approx 2 \rho_0$). Figure 16 shows the symmetry surface incompressibility. We noticed that SKxs25 is nearly independent of density, SKT9 is highly decreasing, and NRAPR again has an inflection point at $\rho \approx 1.8 \rho_0$. Figure 17 shows the effect of asymmetry parameter X on the surface energy. The main surface properties are presented in Table 3.

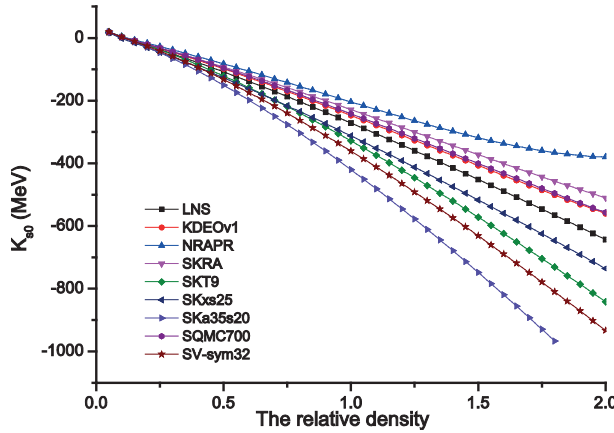


Figure 15. The dependence of bulk surface incompressibility on relative density (ρ / ρ_0) for some Skyrme parameterizations.

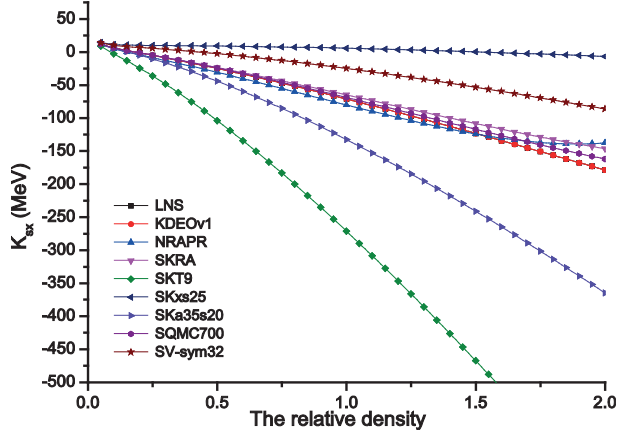


Figure 16. The dependence of symmetry surface incompressibility on relative density (ρ / ρ_0) for some Skyrme parameterizations.

3.3. Curvature properties

3.3.1. Curvature energy

Figure 18 shows the behavior of the bulk curvature energy with the relative density for some Skyrme parameterizations. We note that the bulk curvature energy increases with density, reaches its maximum value ($E_{c0} \approx 15$ MeV) at a relative density $\rho \approx 0.25 \rho_0$, and then decreases to reach its zero value at $\rho \approx 2 \rho_0$. Figure 19 shows the symmetry curvature energy for some Skyrme parameterizations. We note that the symmetry curvature energy increases with density, reaches its maximum value ($E_{cx} \approx 15$ MeV) at a relative density $\rho \approx 0.2 \rho_0$, and then decreases to reach its zero value at $\rho \approx 0.65 \rho_0$. Figure 20 shows the dependence of the curvature energy on the asymmetry parameter X for LNS parameterization. We note that for densities $\rho \leq \rho_0$ the curvature energy is almost independent of the asymmetry parameter.

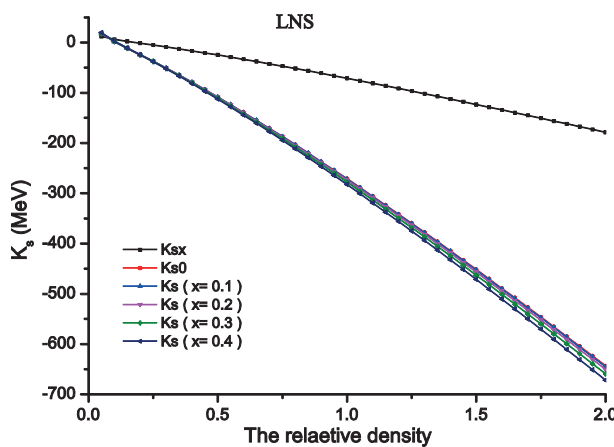


Figure 17. The effect of asymmetry parameter X on surface incompressibility for LNS parameterization.

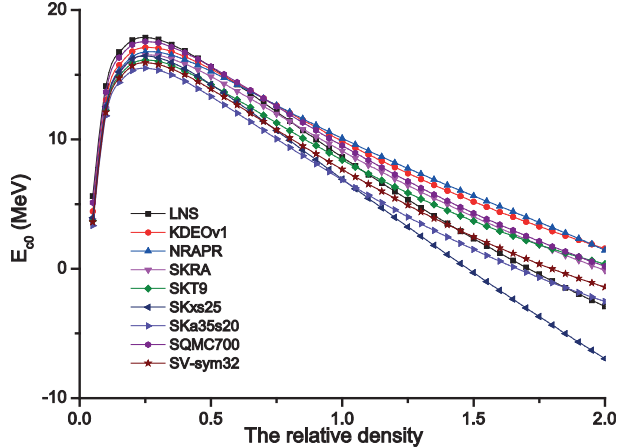


Figure 18. The dependence of bulk curvature energy on relative density (ρ / ρ_0) for some Skyrme parameterizations.

Table 3. The main surface properties of ASINM at saturation for different Skyrme parameterizations.

Skyrme force	E_{S0}	E_{Sx}	L_{S0}	L_{Sx}	K_{S0}	K_{Sx}	Q_{S0}	Q_{Sx}
BSK3	18.90	31.58	-64.20	-32.01	-452.5	-281.2	711.1	296.2
BSK6	18.29	-27.19	15.11	-38.85	-294.0	-369.4	673.0	696.7
BSK16	18.81	-5.11	13.05	-68.81	-323.1	-268.0	682.9	545.2
BSK17	18.95	-4.72	13.50	-65.27	-322.9	-259.2	682.5	527.1
KDEOV	18.21	-27.99	48.06	-108.92	-229.7	-280.2	694.4	838.5
MSK5	18.63	-2.56	-50.49	-105.18	-418.4	-386.0	709.7	701.5
MSK6	18.73	-1.32	-50.10	-97.73	-418.1	-371.1	709.2	671.7
MSL0	18.81	21.94	16.52	36.44	-291.4	-33.9	680.9	-39.9
SK255	19.17	49.29	11.21	126.54	-352.0	92.6	677.8	-379.0
SK272	19.07	40.23	15.53	100.16	-380.9	42.0	634.1	-235.4
SKa25s20	18.60	12.31	-34.01	8.05	-363.3	-126.7	728.8	238.7
SKa35s20	18.65	13.67	-42.81	11.09	-420.2	-132.5	709.0	197.0
SKI3	18.16	-81.07	118.37	-131.92	-127.6	-213.8	1474.1	2015.0
SKI4	17.99	-54.15	76.08	-120.79	-212.1	-265.4	799.5	1053.9
SKM*	17.95	28.20	24.20	24.16	-201.7	-74.1	672.4	17.2
SKMP	17.96	10.18	77.31	29.22	-180.0	-4.3	761.3	18.6
SKP	19.26	47.07	-31.45	18.89	-196.6	-143.0	729.1	63.0
SKSC6	19.63	-6.09	-39.09	-91.64	-411.9	-304.6	714.3	548.4
SKT1	19.64	9.77	-39.29	-6.53	-412.9	-154.5	716.3	248.0
SKT2	19.67	9.77	-39.01	-6.45	-412.2	-154.2	714.9	247.5
SKT3	19.63	10.37	-39.15	-3.88	-412.3	-151.1	715.0	241.4
SKT9	19.20	-7.85	5.21	-75.67	-328.2	-271.1	687.4	572.3
SKX	18.65	46.85	-47.75	33.17	-497.7	-166.3	619.1	-40.4
SKXce	18.60	48.09	-49.81	41.04	-498.3	-135.2	614.7	-95.2
SKXm	18.51	42.21	-34.92	23.04	-401.0	-157.7	708.3	57.7
SKxs20	18.40	18.52	-25.09	21.93	-311.9	-105.1	710.9	199.2
SKxs25	18.78	29.32	-22.84	84.36	-310.2	5.7	708.8	-82.3
SLY6	18.14	-44.73	59.79	-135.57	-210.2	-297.6	703.6	1004.8
SQMC650	19.44	38.51	35.25	43.91	-254.6	-73.0	683.3	-24.2
SV-MIN	18.63	8.43	-27.23	-21.41	-356.1	-177.5	718.6	336.3
vo70	18.46	58.92	-50.83	6.69	-418.1	-231.2	709.6	62.6
KDEOV1	18.70	-25.86	38.73	94.21	-247.3	-260.1	699.9	782.4
LNS	16.59	21.58	8.47	22.72	-271.2	-71.1	685.9	57.0
NPAPR	17.17	16.58	56.92	11.11	-204.2	-80.1	698.3	128.7
SKRA	17.76	25.79	36.54	26.34	-228.5	-64.9	665.1	25.4
SQMC700	18.04	27.49	36.92	31.62	-242.5	-68.9	677.0	26.7
SV-SYM32	18.69	45.22	-16.23	73.29	-360.8	-24.9	700.3	-178.2

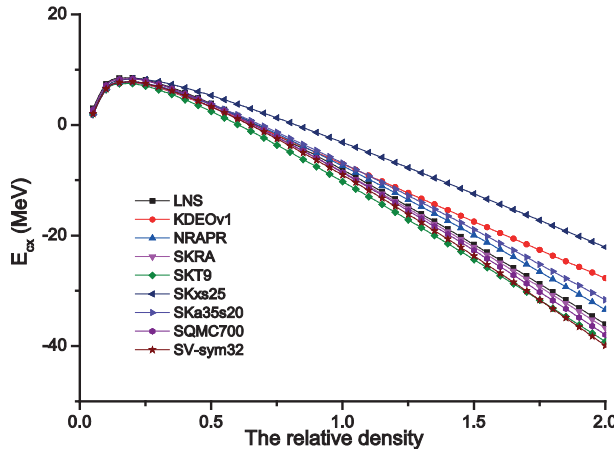


Figure 19. The dependence of symmetry curvature energy on relative density (ρ / ρ_0) for some Skyrme parameterizations.

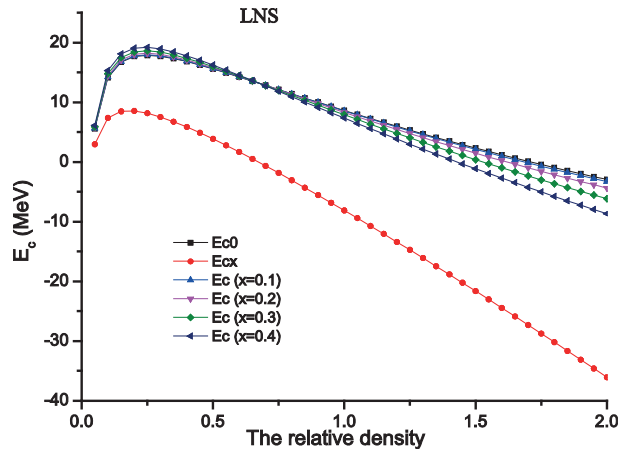


Figure 20. The effect of asymmetry parameter X on curvature energy for LNS parameterization.

3.3.2. Curvature pressure

Figure 21 shows the bulk curvature pressure for some Skyrme parameterizations. It decreases monotonically with density, reaches its zero value at $\rho \approx \rho_0$, and then becomes negative. Figure 22 shows the symmetry curvature pressure that always gets negative values.

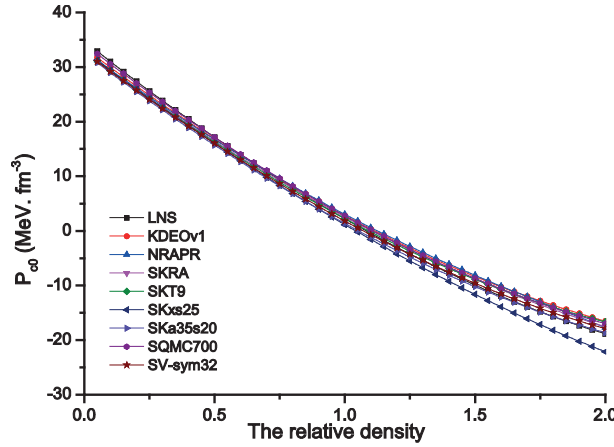


Figure 21. The dependence of bulk curvature pressure on relative density (ρ / ρ_0) for some Skyrme parameterizations.

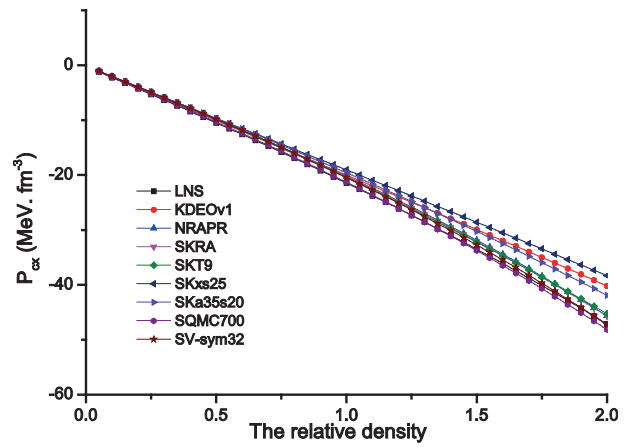


Figure 22. The dependence of symmetry curvature pressure on relative density (ρ / ρ_0) for some Skyrme parameterizations.

3.3.3. Curvature incompressibility

Figure 23 shows the bulk curvature incompressibility for some Skyrme parameterizations. Figure 24 shows the symmetry curvature incompressibility for some Skyrme parameterizations. Figure 25 shows the effect of the asymmetry parameter X on the curvature incompressibility for LNS parameterization. The curvature incompressibility is almost independent of the symmetry parameter. Table 4 shows the main curvature properties at saturation.

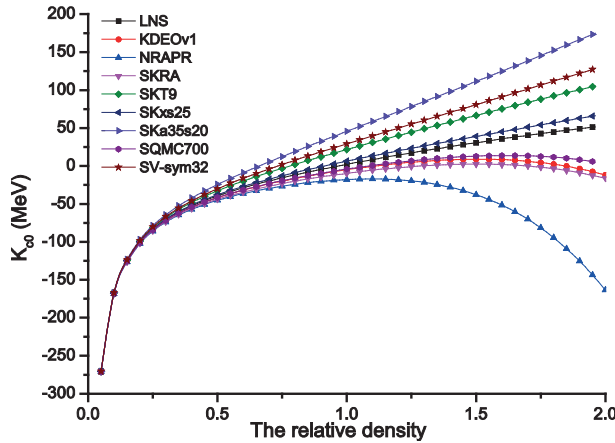


Figure 23. The dependence of bulk curvature incompressibility on relative density (ρ / ρ_0) for some Skyrme parameterizations.

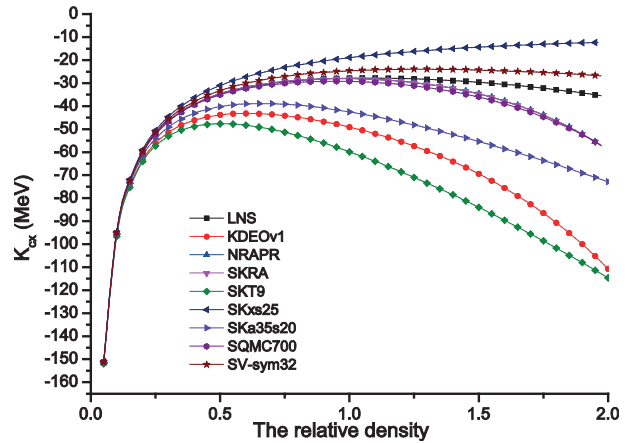


Figure 24. The dependence of symmetry curvature incompressibility on relative density (ρ / ρ_0) for some Skyrme parameterizations.

3.4. Semiinfinite nuclear matter properties

We studied the effect of asymmetry parameter X on the main properties of the semiinfinite nuclear matter system (uncharged spherical nucleus with mass number A). Figure 26 shows the effect of the asymmetry parameter X on the total energy per nucleon of the system. The total energy is highly increasing by increasing the asymmetry parameter. Figure 27 shows the effect of the asymmetry parameter X on the total pressure of the system. For a nucleus with mass number $A < 26$ the total pressure decreases with increasing asymmetry parameter, while it increases at $A > 26$. For $A = 26$ the pressure is independent of the asymmetry parameter. The total pressure of systems with $A \leq 75$ increases rapidly with mass number, while it increases slowly for system with $A > 100$. Figure 28 shows the effect of asymmetry parameter X on the incompressibility of the system. The incompressibility of the system decreases with increase of the asymmetry parameter X . We note that for systems with $A \leq 75$ the incompressibility increases rapidly with mass number, while for $A > 100$ it increases slowly.

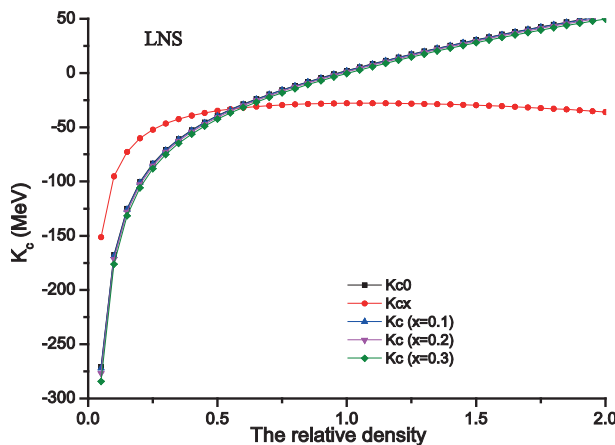


Figure 25. The effect of asymmetry parameter X on curvature incompressibility for LNS parameterization.

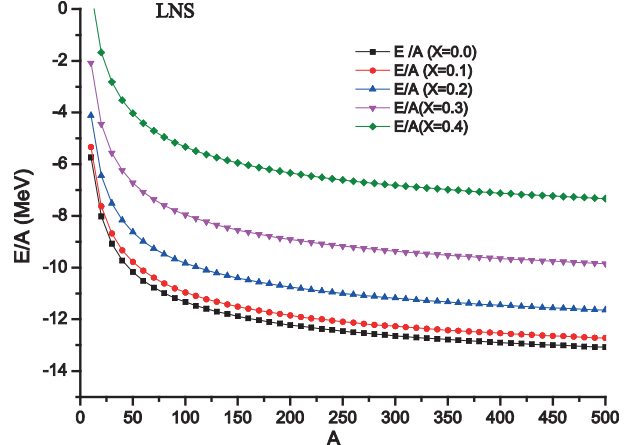


Figure 26. The effect of asymmetry parameter X on total energy per nucleon of the system for LNS parameterization.

Table 4. The main curvature properties of ASINM at saturation for different Skyrme parameterizations.

Skyrme force	E_{C0}	E_{Cx}	L_{C0}	L_{Cx}	K_{C0}	K_{Cx}	Q_{C0}	Q_{Cx}
BSK3	5.85	-17.40	57.83	-37.20	51.7	-68.1	123.0	306.3
BSK6	8.49	-11.70	39.16	-53.48	11.5	-69.3	129.5	220.7
BSK16	8.83	-10.15	42.24	-37.98	21.6	-61.2	114.3	224.5
BSK17	8.82	-9.85	42.21	-36.79	21.6	-59.9	114.5	221.7
KDE	8.33	-7.45	32.18	-43.61	-9.1	-52.4	156.2	157.7
KDEO	9.91	-7.95	31.99	-42.77	-9.7	-52.4	82.0	128.3
KDEOV	9.94	-7.96	32.05	-42.84	-9.7	-52.5	81.4	128.0
MSK5	6.28	-15.70	54.03	-52.92	42.6	-81.3	127.5	280.9
MSK6	6.27	-15.21	53.99	-50.86	42.5	-79.0	127.6	276.2
MSL0	8.62	-6.11	39.16	-5.77	9.8	-25.8	131.5	189.6
SK255	9.02	-3.97	44.86	13.04	32.7	-7.5	101.2	178.2
SK272	9.33	-4.19	46.72	5.96	48.4	-16.0	80.7	180.5
SKa25s20	6.97	-7.07	48.79	-18.49	23.4	-36.6	143.7	190.6
SKa35s20	6.87	-6.96	53.95	-18.36	45.6	-42.5	119.3	198.6
SKI3	11.87	6.61	21.73	-37.85	-88.4	-99.6	-1457.1	-1832.5
SKI4	10.97	-0.56	29.20	-41.83	-19.0	-68.9	-195.2	-196.1
SKM*	8.67	-9.65	35.52	-11.35	-2.4	-28.6	146.0	218.5
SKMP	10.39	-2.96	25.70	-3.07	-28.7	-32.9	-139.8	90.5
SKP	6.72	-16.55	45.64	-20.24	8.0	-33.9	171.3	269.9
SKSC6	6.93	-12.99	53.56	-43.07	42.5	-68.9	121.5	252.6
SKT1	6.96	-7.90	53.71	-21.89	42.7	-45.3	121.1	205.3
SKT2	6.94	-7.90	53.62	-21.86	42.6	-45.2	121.3	205.2
SKT3	6.95	-7.79	53.63	-21.49	42.6	-44.8	121.3	204.2
SKT9	8.41	-10.29	43.37	-38.89	21.7	-59.8	123.7	222.8
SKX	6.97	-14.06	60.22	-19.95	82.3	-56.6	97.7	277.4
SKXce	6.78	-13.55	60.30	-16.14	82.5	-50.2	99.2	270.4
SKXm	7.14	-14.15	51.90	-20.63	40.3	-45.7	121.4	269.3
SKxs20	6.82	-7.43	43.54	-15.66	6.3	-30.0	170.3	186.5
SKxs25	6.84	-3.19	43.24	-10.69	6.0	-18.9	170.3	160.2
SLY6	10.11	-5.70	29.42	-46.09	-15.9	-56.4	23.5	38.8
SQMC650	9.40	-10.82	36.28	-10.88	-1.4	-29.0	132.6	232.8
SV-MIN	7.18	-9.30	47.79	-25.93	23.2	-43.7	140.6	210.2
Vo70	6.28	-21.04	53.99	-29.66	42.5	-57.1	127.6	338.2
KDEOV1	9.86	-7.06	34.70	-40.10	-5.0	-49.1	111.9	140.9
LNS	8.63	-8.11	38.89	-11.42	2.2	-27.8	146.7	198.2
NPAPR	10.08	-7.43	28.99	-12.96	-17.8	-33.4	37.3	178.5
SKRA	9.10	-8.56	32.10	-10.20	-9.7	-28.1	130.3	207.8
SQMC700	9.55	-8.71	34.47	-10.80	-4.1	-29.3	120.0	209.5
SV-SYM32	7.68	-9.14	47.36	-3.13	29.2	-24.6	126.3	221.1

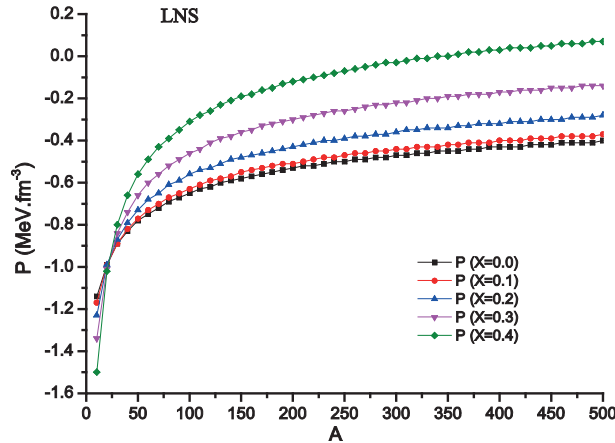


Figure 27. The effect of asymmetry parameter X on total pressure of the system for LNS parameterization.

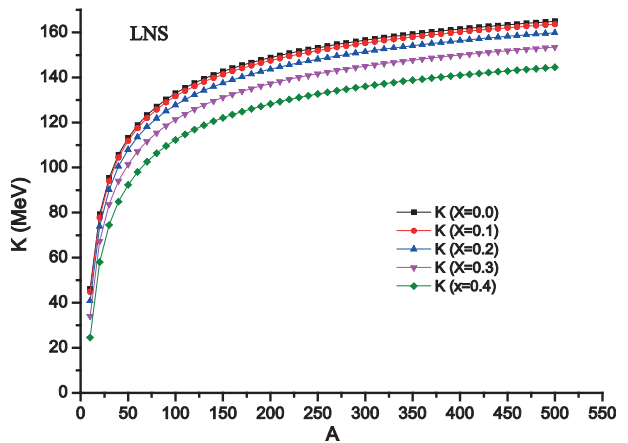


Figure 28. The effect of asymmetry parameter X on incompressibility of the system for LNS parameterization.

4. Summary and conclusions

In the present work, we used a leptodermous expansion for the density profile and got a LDM analytical formula for the energy of an ASINM. We used these formulae to study the volume, surface, and curvature properties (energy, pressure, and incompressibility) of the system. We applied this study to a wide range of Skyrme parameterizations. The bulk volume, bulk surface, and bulk curvature properties for all Skyrme parameterizations under consideration showed the same behavior with density and asymmetry parameter X , with small differences at saturation density. We noticed that all Skyrme parameterizations have a minimum bulk volume pressure at $\rho \approx 0.65 \rho_0$. We also noticed that for densities $\rho \leq 0.65 \rho_0$ the bulk surface pressure is zero and bulk volume incompressibility has the same value for all Skyrme parameterizations. The value of the symmetry volume energy slope (L_{vx}) at saturation reflects the behavior of the symmetry volume, symmetry surface, and symmetry curvature properties of the ASINM. A value of $L_{vx} = 59 \pm 13$ MeV [26,27,33] gives an accepted and consistent behavior of these properties with density. We also studied the effect of asymmetry parameter X on the volume, surface, and curvature properties.

References

- [1] Brown, B. A. *Phys. Rev. Lett.* **2000**, *85*, 5296-5299.
- [2] Lattimer, J. M.; Prakash, M. *Astrophys. J.* **2001**, *550*, 426-422.
- [3] Baran, V.; Colonna, M.; Di Toro, M.; Zielinska-Pfabé, M.; Wolter, H. H. *Phys. Rev. C* **2005**, *72*, 064620.
- [4] Myers, W. D.; Swiatecki, W. J. *Ann. Phys.* **1969**, *55*, 396-505.
- [5] Myers, W. D.; Swiatecki, W. J. *Ann. Phys.* **1974**, *84*, 186-210.
- [6] Myers, W. D.; Swiatecki, W. J. *Nucl. Phys. A* **1996**, *601*, 141-167.
- [7] Myers, W. D.; Swiatecki, W. J. *Phys. Rev. C* **1998**, *57*, 3020-3025.
- [8] Brack, M.; Guet, C.; Hakansson, H. B. *Phys. Reports* **1985**, *123*, 275-346.
- [9] Bartel, J.; Brack, M.; Durand, M. *Nucl. Phys. A* **1985**, *445*, 263-303.
- [10] Brack, M. *Phys. Rev. Lett.* **1984**, *53*, 119-121.
- [11] Brack, M.; Quentin, P. *Phys. Lett. B* **1974**, *52*, 159-162.

- [12] Sauer, G.; Chandra, H.; Mosel, U. *Nucl. Phys. A* **1976**, *264*, 221-243.
- [13] Abd-Alla, M. *Proc. Math. Soc. Egypt* **2006**, *84*, 169-191.
- [14] Ramadan, S.; Abd-Alla, M.; Hassan, M. Y. M. *Phys. Rev. C* **1996**, *53*, 1670-1683.
- [15] Uma Maheswari, V. S.; Ramamurthy, V. S.; Satpathy, L. *Phys. Rev. C* **1995**, *52*, 1431-1442.
- [16] Kolomietz, V. M.; Sanzhur, A. I.; Shlomo, S.; Firin, S. A. *Phys. Rev. C* **2001**, *64*, 24315-24316.
- [17] Bondorf, J. P.; Donangelo, R.; Mishustin, I. N.; Pethick, C. J.; Schulz, K.; Sneppen, H. *Nucl. Phys. A* **1985**, *443*, 321-347.
- [18] Hoel, C.; Sobotka, L. G.; Charity, R. J. *Phys. Rev. C* **2007**, *75*, 17601-17602.
- [19] Blin, A. H.; Brack, M. *Nucl. Phys. A* **1989**, *504*, 300-322.
- [20] Srivastava, D. K. *Phys. Lett. B* **1982**, *112*, 289-291.
- [21] Abd-Alla, M. *Acta Phys. Pol. B* **1992**, *23*, 807-814.
- [22] Wang, N.; Liu, M.; Jiang, H.; Tian, J. L.; Zhao, Y. M. *Phys. Rev. C* **2015**, *91*, 044308.
- [23] Seif, W. M.; Basu, D. N. *Phys. Rev. C* **2014**, *89*, 028801.
- [24] Dutra, L.; Lourenco, O.; Sa Martins, J. S.; Del?no, A.; Stone, J. R.; Stevenson, P. D. *Phys. Rev. C* **2012**, *85*, 035201.
- [25] Cherevko, K. V.; Bulavin, L. A.; Jenkovszky, L. L.; Syssoev, V. M.; Zhang, F. S. *Phys. Rev. C* **2015**, *92*, 014308.
- [26] Jiang, H.; Fu, G. J.; Zhao, Y. M.; Arima, A. *Phys. Rev. C* **2012**, *85*, 024301.
- [27] Agrawal, B. K.; De, J. N.; Samaddar, S. K. *Phys. Rev. Lett.* **2012**, *109*, 262501.
- [28] Agrawal, B. K.; De, J. N.; Samaddar, S. K.; Colo, G.; Sulaksono, A. *Phys. Rev. C* **2013**, *87*, 051306.
- [29] Liu, J.; Ren, Z.; Xu, C.; Xu, R. *Phys. Rev. C* **2013**, *88*, 024324.
- [30] Mondal, C.; Agrawal, B. K.; De, J. N. *Phys. Rev. C* **2015**, *92*, 024302.
- [31] Reinhard, P. G.; Bender, M.; Nazarewicz, W.; Vertse, T. *Phys. Rev. C* **2006**, *73*, 014309.
- [32] Royer, G. *Nucl. Phys. A* **2008**, *807*, 105-116.
- [33] Roca-Maza, X.; Colo, G.; Sagawa, H. *Phys. Rev. C* **2012**, *86*, 031306.
- [34] Abd-Alla, M. *Acta Phys. Pol. B* **2003**, *34*, 189-212.
- [35] Samyn, M.; Goriely, S.; Pearson, J. M. *Nucl. Phys. A* **2003**, *725*, 69-81.
- [36] Goriely, S.; Samyn, M.; Bender, M.; Pearson, J. M. *Phys. Rev. C* **2003**, *68*, 054325.
- [37] Chamel, N.; Goriely, S.; Pearson, J. M. *Nucl. Phys. A* **2008**, *812*, 72-98.
- [38] Goriely, S.; Chamel, N.; Pearson, J. M. *Phys. Rev. Lett.* **2009**, *102*, 152503-152507.
- [39] Agrawal, B. K.; Shlomo, S.; Kim Au, V. *Phys. Rev. C* **2005**, *72*, 014310.
- [40] Tondeur, F.; Goriely, S.; Pearson, J. M.; Onsi, M. *Phys. Rev. C* **2000**, *62*, 024308.
- [41] Chen, L. W.; Ko, C. M.; Li, B. A.; Xu, J. *Phys. Rev. C* **2010**, *82*, 024321.
- [42] Agrawal, B. K.; Shlomo, S.; Kim Au, V. *Phys. Rev. C* **2003**, *68*, 031304.
- [43] Reinhard, P. G.; Flocard, H. *Nucl. Phys. A* **1995**, *584*, 467-488.
- [44] Bennour, L.; Heenen, P. H.; Bonche, P.; Dobaczewski, J.; Flocard, H. *Phys. Rev. C* **1989**, *40*, 2834-2839.
- [45] Dobaczewski, J.; Flocard, H.; Treiner, J. *Nucl. Phys. A* **1984**, *422*, 103-139.
- [46] Onsi, M.; Przysiezniak, H.; Pearson, J. M. *Phys. Rev. C* **1994**, *50*, 460-468.
- [47] Tondeur, F.; Brack, M.; Farine, M.; Pearson, M. *Nucl. Phys. A* **1984**, *420*, 297-319.

- [48] Brown, B. A. *Phys. Rev. C* **1998**, *58*, 220-231.
- [49] Brown, B. A.; Shen, G.; Hillhouse, G. C.; Meng, J.; Trzcinska, A. *Phys. Rev. C* **2007**, *76*, 034305.
- [50] Chabanat, E.; Bonche, P.; Haensel, R.; Meyer, J.; Schaeffer, R. *Nucl. Phys. A* **1998**, *635*, 231-256.
- [51] Goriely, S.; Samyn, M.; Pearson, J. M. *Phys. Rev. C* **2007**, *75*, 064312.
- [52] Rashdan, M. *Mod. Phys. Lett. A* **2000**, *15*, 1287-1300.
- [53] Cao, L. G.; Lombardo, U.; Shen, C. W.; Van Giai, N. *Phys. Rev. C* **2006**, *73*, 014313.
- [54] Steiner, A. W.; Prakash, M.; Lattimer, J. M.; Ellis, P. J. *Phys. Rep.* **2005**, *411*, 325-357.
- [55] Pearson, J. M.; Goriely, S. *Phys. Rev. C* **2001**, *64*, 027301.
- [56] Klupfel, P.; Reinhard, P. G.; Burvenich, T. J.; Maruhn, J. A. *Phys. Rev. C* **2009**, *79*, 034310.

Appendix

The bulk surface energy E_{s0} is:

$$\begin{aligned}
E_{s0} = & -\left(\frac{3d}{r_0}\right) \left\{ \frac{3}{8}t_0\rho B_s(2) + \frac{1}{16}t_3\rho^{\alpha+1}B_s(\alpha+2) + \left(\frac{v}{d}\right)^2 \rho C G_1(0) \right\} \\
& -\left(\frac{3v}{r_0}\right)\frac{\hbar^2}{2m} \left\{ \begin{array}{l} \left(\frac{3d}{5v}\right)(1.5\pi^2\rho)^{\frac{2}{3}} B_s(\frac{5}{3}) + \frac{1}{3d}B_{d1} \\ +\left(\frac{v}{d}\right) \left[\begin{array}{l} \frac{1}{36}G_1(-1) + \frac{C\rho}{6}G_1(0) - \left(\frac{C\rho}{2}\right)^2 G_1(1) \\ \frac{1}{3}(C\rho)^3 G_1(2) - \frac{5}{12}(C\rho)^4 G_1(3) + \frac{5}{12}(C\rho)^5 G_1(4) \end{array} \right] \\ \left(\frac{C\rho}{6}\right) [F_1(5) - C\rho F_1(2) + (C\rho)^2 F_1(3) - (C\rho)^3 F_1(4)] \end{array} \right\} \\
& -\frac{1}{6480}\frac{\hbar^2}{2m} (1.5\pi^2\rho)^{-\frac{2}{3}} \left(\frac{3d}{r_0}\right) C_2 \left\{ 8\left(\frac{v}{d}\right)^4 H_1 - 27\frac{q^3}{d^4}Q_1 + 24\frac{q^3}{d^4}P_1 \right\} \\
& -\left(\frac{3v}{r_0}\right)C_2\rho \left\{ \begin{array}{l} -\frac{11}{36}G_1(0) + \left(\frac{C\rho}{6}\right) G_1(1) \\ \frac{3d}{5v} \left(\frac{3\pi^2\rho}{2}\right)^{\frac{2}{3}} B_s(\frac{8}{3}) + \left(\frac{v}{d}\right) \left[\begin{array}{l} -\left(\frac{C\rho}{2}\right)^2 G_1(2) + \frac{1}{3}(C\rho)^3 G_1(3) \\ -\frac{5}{12}(C\rho)^4 G_1(4) + \frac{5}{12}(C\rho)^5 G_1(5) \end{array} \right] \\ \frac{C\rho}{6} [F_1(2) - (C\rho)F_1(3) + (C\rho)^2 F_1(4) - (C\rho)^3 F_1(5)] \end{array} \right\} \\
& -\frac{1}{6480} \left(\frac{2}{3\pi^2}\right)^{\frac{2}{3}} \left(\frac{3d}{r_0}\right) C_2\rho^{\frac{1}{3}} \left\{ -7\left(\frac{v}{d}\right)^4 H_2 - \frac{3v^3}{d^4}Q_2 + \frac{30v^2}{d^4}P_2 \right\}
\end{aligned} \tag{23}$$

The surface symmetry energy E_{sx} is:

$$\begin{aligned}
E_{sx} = & \frac{3d}{r_0} \left\{ \begin{array}{l} \frac{1}{8}t_0\rho B_s(2)(1+2x_0) + \frac{1}{48}t_3\rho^{\alpha+1}B_s(\alpha+2)(1+2x_3) \\ + \left(\frac{v}{a}\right)^2 \rho C_3 G_1(0) \end{array} \right\} \\
& -\frac{5v}{3r_0}\frac{\hbar^2}{2m} \left\{ \begin{array}{l} \left(\frac{3d}{5v}\right)(1.5\pi^2\rho)^{\frac{2}{3}} B_s(\frac{5}{3}) + \frac{1}{3d}B_{d1} \\ +\left(\frac{v}{d}\right) \left[\begin{array}{l} \frac{1}{36}G_1(-1) + \frac{C_3\rho}{6}G_1(0) - \left(\frac{C_3\rho}{2}\right)^2 G_1(1) \\ \frac{1}{3}(C_3\rho)^3 G_1(2) - \frac{5}{12}(C_3\rho)^4 G_1(3) + \frac{5}{12}(C_3\rho)^5 G_1(4) \end{array} \right] \\ \left(\frac{C_3\rho}{6}\right) [F_1(1) - C_3\rho F_1(2) + (C_3\rho)^2 F_1(3) - (C_3\rho)^3 F_1(4)] \end{array} \right\}
\end{aligned}$$

$$\begin{aligned}
& -\frac{1}{6480} \frac{\hbar^2}{2m} (1.5\pi^2\rho)^{-\frac{2}{3}} \left(\frac{5d}{3r_0} \right) C_4 \left\{ 8 \left(\frac{v}{d} \right)^4 H_1 - 27 \frac{q^3}{d^4} Q_1 + 24 \frac{q^3}{d^4} P_1 \right\} \\
& - \left(\frac{3v}{r_0} \right) C_4 \rho \left\{ \begin{array}{l} \left[\begin{array}{l} -\frac{11}{36} G_1(0) + \left(\frac{C\rho}{6} \right) G_1(1) \\ - \left(\frac{C\rho}{2} \right)^2 G_1(2) + \frac{1}{3} (C\rho)^3 G_1(3) \\ -\frac{5}{12} (C\rho)^4 G_1(4) + \frac{5}{12} (C\rho)^5 G_1(5) \end{array} \right] \\ \frac{C\rho}{6} [F_1(2) - (C\rho) F_1(3) + (C\rho)^2 F_1(4) - (C\rho)^3 F_1(5)] \end{array} \right\} \\
& - \frac{1}{6480} \left(\frac{2}{3\pi^2} \right)^{\frac{2}{3}} \left(\frac{3d}{r_0} \right) C_4 \rho^{\frac{1}{3}} \left\{ -7 \left(\frac{v}{d} \right)^4 H_2 - \frac{3v^3}{d^4} Q_2 + \frac{30v^2}{d^4} P_2 \right\} \quad (24)
\end{aligned}$$

The bulk curvature energy is:

$$\begin{aligned}
E_{c0} &= \left(\frac{6d}{r_0} \right)^2 \left\{ \frac{3}{8} t_0 \rho B_c(2) + \frac{1}{16} t_3 \rho^{\alpha+1} B_c(\alpha+2) + \left(\frac{v}{d} \right)^2 \rho C B_c(0) \right\} \\
& + \left(\frac{6dv}{r_0^2} \right) \frac{\hbar^2}{2m} \left\{ \begin{array}{l} \left(\frac{3d}{5v} \right) (1.5\pi^2\rho)^{\frac{2}{3}} B_c(\frac{5}{3}) \\ + \left(\frac{v}{d} \right) \left[\begin{array}{l} \frac{1}{36} B_c(-1) + \frac{C\rho}{6} B_c(0) - \left(\frac{C\rho}{2} \right)^2 B_c(1) \\ \frac{1}{3} (C\rho)^3 B_c(2) - \frac{5}{12} (C\rho)^4 B_c(3) + \frac{5}{12} (C\rho)^5 B_c(4) \end{array} \right] \\ \left(\frac{C\rho}{6} \right) [X(1) - C\rho X(2) + (C\rho)^2 X(3) - (C\rho)^3 X(4)] \end{array} \right\} \\
& + \frac{6}{6480} \frac{\hbar^2}{2m} (1.5\pi^2\rho)^{-\frac{2}{3}} \left(\frac{d}{r_0} \right)^2 \left\{ \begin{array}{l} 8 \left(\frac{v}{d} \right)^4 [H_2 - H_1 A_1(v) - 27 \frac{q^3}{d^4} [Q_2 - Q_1 A_1(v)] \\ + 24 \frac{q^3}{d^4} [P_2 - P_1 A_1(v)] \end{array} \right\} \\
& + \frac{1}{6480} \left(\frac{2}{3\pi^2} \right)^{\frac{2}{3}} \frac{\hbar^2}{2m} \left(\frac{8\pi r_0 v^2}{d^3} \right) \rho^{\frac{1}{3}} \left\{ \begin{array}{l} 24 \left[\begin{array}{l} (v+1) A_1(\frac{v+9}{3}) - (3v+2) A_1(\frac{v+6}{3}) \\ +(3v+1) A_1(\frac{v+3}{3}) - v A_1(v) \end{array} \right] \\ -27v \left[\begin{array}{l} A_1(\frac{v+9}{3}) - 3A_1(\frac{v+6}{3}) \\ +3A_1(\frac{v+3}{3}) - A_1(v) \end{array} \right] \end{array} \right\} \quad (26)
\end{aligned}$$

The curvature symmetry energy is:

$$\begin{aligned}
E_{cx} = & \left(\frac{6d}{r_0} \right)^2 \left\{ \frac{1}{8} t_0 \rho B_c(2)(1+2x_0) + \frac{1}{48} t_3 \rho^{\alpha+1} B_c(\alpha+2)(1+2x_3) + \left(\frac{v}{d} \right)^2 \rho C B_c(0) \right\} \\
& + \left(\frac{6dv}{r_0^2} \right) \frac{\hbar^2}{2m} \left\{ \begin{array}{l} \left(\frac{d}{3v} \right) (1.5\pi^2\rho)^{\frac{2}{3}} B_c(\frac{5}{3}) \\ + \left(\frac{v}{d} \right) \left[\begin{array}{l} \frac{1}{36} B_c(-1) + \frac{C\rho}{6} B_c(0) - \left(\frac{C\rho}{2} \right)^2 B_c(1) \\ \frac{1}{3}(C\rho)^3 B_c(2) - \frac{5}{12}(C\rho)^4 B_c(3) + \frac{5}{12}(C\rho)^5 B_c(4) \end{array} \right] \\ \left(\frac{C\rho}{6} \right) [X(1) - C\rho X(2) + (C\rho)^2 X(3) - (C\rho)^3 X(4)] \end{array} \right\} \\
& + \frac{6}{6480} \frac{\hbar^2}{2m} (1.5\pi^2\rho)^{-\frac{2}{3}} \left(\frac{d}{r_0} \right)^2 \left\{ \begin{array}{l} 8 \left(\frac{v}{d} \right)^4 [H_2 - H_1 A_1(v) - 27 \frac{q^3}{d^4} [Q_2 - Q_1 A_1(v)] \\ + 24 \frac{q^3}{d^4} [P_2 - P_1 A_1(v)] \end{array} \right\} \\
& + \frac{1}{6480} \left(\frac{2}{3\pi^2} \right)^{\frac{2}{3}} \frac{\hbar^2}{2m} \left(\frac{8\pi r_0 v^2}{d^3} \right) \rho^{\frac{1}{3}} \left\{ \begin{array}{l} 24 \left[\begin{array}{l} (v+1) A_1(\frac{v+9}{3}) - (3v+2) A_1(\frac{v+6}{3}) \\ +(3v+1) A_1(\frac{v+3}{3}) - v A_1(v) \end{array} \right] \\ - 27v \left[\begin{array}{l} A_1(\frac{v+9}{3}) - 3A_1(\frac{v+6}{3}) \\ + 3A_1(\frac{v+3}{3}) - A_1(v) \end{array} \right] \end{array} \right\} \quad (27)
\end{aligned}$$

The constants C , $C1$, $C2$, $C3$, $B_s(n)$, B_{d1} , $G1(n)$, $F1(n)$, H_1 , H_2 , Q_1 , Q_2 , $P1$, $P2$, $B_c(n)$, B_c , and $X(n)$ are related to the coefficients $A_n(m)$ and are given in reference [34].